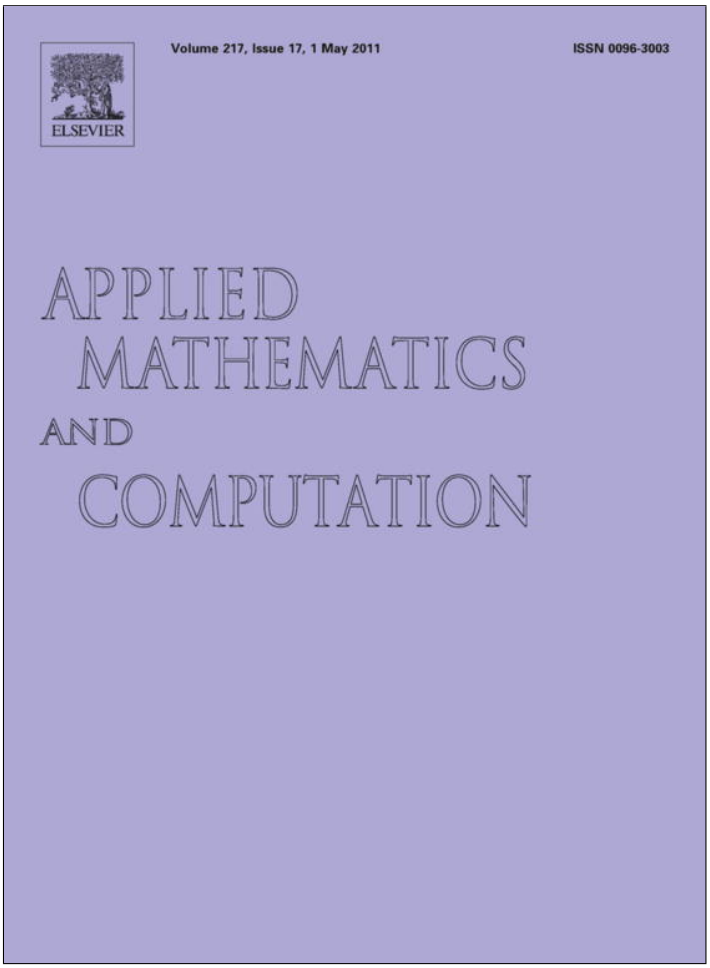

Applied Mathematics and Computation 217 (2011) 7092–7107

Contents lists available at ScienceDirect

Applied Mathematics and Computation

journal homepage: www.elsevier.com/locate/amc

Stieltjes representation of the 3D Bruggeman effective medium and Padé approximation

Dali Zhang [a,*], Elena Cherkaev [b], Michael P. Lamoureux [a]

[a] University of Calgary, Department of Mathematics and Statistics, 2500 University Drive NW, Calgary, Alberta, Canada T2N 1N4
[b] University of Utah, Department of Mathematics, 155 South 1400 East, JWB 233, Salt Lake City, UT 84112, USA

ARTICLE INFO

Keywords:
Bruggeman self-consistent effective medium approximation
Spectral density function
Stieltjes representation
Padé approximation
Effective complex permittivity
Two-phase composite

ABSTRACT

The paper deals with Bruggeman effective medium approximation (EMA) which is often used to model effective complex permittivity of a two-phase composite. We derive the Stieltjes integral representation of the 3D Bruggeman effective medium and use constrained Padé approximation method introduced in [39] to numerically reconstruct the spectral density function in this representation from the effective complex permittivity known in a range of frequencies. The problem of reconstruction of the Stieltjes integral representation arises in inverse homogenization problem where information about the spectral function recovered from the effective properties of the composite, is used to characterize its geometric structure. We present two different proofs of the Stieltjes analytical representation for the effective complex permittivity in the 3D Bruggeman effective medium model: one proof is based on direct calculation, the other one is the derivation of the representation using Stieltjes inversion formula. We show that the continuous spectral density in the integral representation for the Bruggeman EMA model can be efficiently approximated by a rational function. A rational approximation of the spectral density is obtained from the solution of a constrained minimization problem followed by the partial fractions decomposition. We show results of numerical rational approximation of Bruggeman continuous spectral density and use these results for estimation of fractions of components in a composite from simulated effective permittivity of the medium. The volume fractions of the constituents in the composite calculated from the recovered spectral function show good agreement between theoretical and predicted values.

1. Introduction

The Bruggeman effective-medium approximation (EMA) [6,22] is one of the mixing rules that is widely used in electromagnetics for modeling the effective response of heterogeneous composite materials. Indeed, many physical phenomena in heterogeneous media can be described by the effective medium theory which gives the effective complex permittivity ϵ^* of a mixture of two materials with complex permittivity ϵ_1 and ϵ_2. The EMA model is based on an assumption that the inhomogeneous material is composed of two types of approximately spherical grains with complex-valued permittivity ϵ_1 and ϵ_2 mixed in the volume fractions f and $1-f$. It was shown that the Bruggeman model of the effective permittivity corresponds to a hierarchical medium with inclusions of very different sizes, so that any two spherical inclusions of similar size are so well separated that the whole assemblage can be viewed as a dilute composite [27,34]. The derivation of the effective permittivity ϵ^* is based on the assumption of self-consistency which allows to replace the material surrounding the inclusions

* Corresponding author.
E-mail addresses: dlzhang@math.ucalgary.ca (D. Zhang), elena@math.utah.edu (E. Cherkaev), mikel@math.ucalgary.ca (M.P. Lamoureux).

0096-3003/$ - see front matter © 2011 Elsevier Inc. All rights reserved.
doi:10.1016/j.amc.2011.01.020

by a homogeneous matrix material with the same effective permittivity $\epsilon^*(f,\epsilon_1,\epsilon_2)$, and use first order approximation for dilute composite to calculate the resulting effective property. This model is also called self-consistent effective medium approximation [23,28,31]. Though the model behind the Bruggeman effective medium formula is relatively simple, this approximation gives a description of percolation phenomenon [18], and this is one of the reasons for its wide use in physics. Indeed, the applications exploiting Bruggeman effective medium formula and spectral representation range from characterization of optical and electrical properties of cermets [21] and modeling linear and nonlinear composites [30,36] to calculation of the effective response of composite polycrystalline and metamaterials [2,35], dielectric properties of biological cells [19], and critical behavior of self-similar brine-filled porous rocks [16].

Spectral representation of the effective complex permittivity of a two-phase composite was introduced in [3] and used to bound the effective permittivity of composites formed from two materials with permittivity ϵ_1 and ϵ_2 [4,17,26]. It presents the effective permittivity ϵ^* as a Stieltjes function with special analytical properties:

$$F(s) = 1 - \frac{\epsilon^*}{\epsilon_2} = \int_0^1 \frac{\mathrm{d}\mu(x)}{s-x}, \quad s = \frac{1}{1-\epsilon_1/\epsilon_2}. \tag{1}$$

Here the positive measure μ is the spectral measure of a self-adjoint operator $\Gamma\chi$, with χ being the characteristic function of the domain occupied by the first material in the composite, and $\Gamma = \nabla(-\Delta)^{-1}(\nabla\cdot)$, where $(-\Delta)$ is the Laplacian operator. The function $F(s)$ is analytic outside the $[0,1]$-interval in the complex s-plane. The representation is valid for other physical properties such as electrical conductivity, thermal conductivity, diffusivity and elastic properties.

The specific feature of the spectral representation (1) is that it separates the dependence of the effective permittivity ϵ^* on the properties of the components from the dependence on the micro-geometry through the complex variable s. This feature of the analytic representation was used to infer information about the microgeometry of the composite [10,12,24,25]. The inverse homogenization method [10] allows to estimate the parameters of the microstructure of a composite using measured effective properties of the medium. The method is based on the reconstruction of the spectral measure in the analytic Stieltjes integral representation (1), the spectral measure contains all information about the microgeometry. It was shown that the spectral measure can be uniquely recovered from the measurements of the effective property over a range of frequencies [10], but the problem of reconstruction is ill-posed and requires regularization. The inverse homogenization was extended to viscoelastic composite media in [7]. Regularized method of constrained rational approximation of the spectral function was developed in [39] and used in [38] for evaluation of microstructural parameters of the composite and in [40] for modeling of wave propagation in viscoelastic medium.

The aim of this paper is to present a derivation of the analytic Stieltjes integral representation for the 3D Bruggeman EMA model which has a continuous spectral density function. Particular cases of the spectral representation for Bruggeman medium or the whole formula have appeared already in several publications [15,21,23,29,32,36]. For instance, Stieltjes representation formula for the case of low volume fraction of the first material (less than threshold value equal 1/3), was used in [15,21,29] to describe results of experiments. The whole formula has appeared in (49–52) of Ref. [23], in (12) and (13) of Ref. [36], and in Table 1 of [32]. However these references did not provide the detailed proof of the spectral representation formula. Here we present two detailed derivations of the Stieltjes integral representation, one proof is based on direct calculation and the second one (in Appendix) is based on application of the Stieltjes inversion formula [37].

In the second part of the paper, we use the derived Stieltjes integral representation to investigate the inverse homogenization problem for Bruggeman composite and to numerically study the efficiency of the constrained Padé approximation method for the case of continuous spectral density in the Bruggeman model. Assuming that the values of the effective complex permittivity are available in an interval of frequencies (which provides necessary and sufficient data to uniquely recover the spectral density function [10]), we use a recently developed constrained Padé approximation method [39] to construct a low order Padé approximation to the continuous spectral function. Padé approximation is constructed solving constrained minimization problem followed by partial fraction decomposition. Constrained minimization algorithm provides regularization of the problem. The resulting approximation consists of small number of poles accurately approximating continuous spectral density. The developed algorithm is applied to the problem of estimation of volume fractions of the constituents in a metal–insulator composite material. The problem of estimation of concentrations or fractions of constituents in the mixture is of significant interest in nondestructive testing of composite materials, it has various biomedical, geophysical, engineering, and material science applications [8,9,12–14,24,25,38,39]. We assume that the effective complex permittivity is given by the 3D Bruggeman EMA analytical model, construct Padé approximation of the spectral function, and calculate the volume fraction of one of the constituents as zero moment of the spectral function. The results show good agreement between theoretical and predicted values and demonstrate the efficiency of the presented method.

The method can be used for constructing an accurate approximation to the 3D Bruggeman effective medium in numerical applications dealing with spectral representation. In particular, it can be used for extraction of the spectral function from effective measurements to use it in prediction of other effective properties of the same composite [10,11] or in prediction of effective properties of a different composite with similar topology [23].

2. Spectral representation of 3D Bruggeman EMA model

This section presents the derivation of an analytic Stieltjes integral representation for the effective permittivity ϵ^* of the three-dimensional (3D) Bruggeman self-consistent effective medium analytic model which has a continuous spectral density

function. In 3D Bruggeman's symmetric EMA model, the self-consistency condition results in the equation relating the effective permittivity ϵ^* of a two-phase mixture with permittivity and fractions of the components:

$$f\frac{\epsilon^*-\epsilon_1}{2\epsilon^*+\epsilon_1}+(1-f)\frac{\epsilon^*-\epsilon_2}{2\epsilon^*+\epsilon_2}=0. \tag{2}$$

Here f is the volume fraction of the first phase with permittivity ϵ_1, and $1-f$ is the volume fraction of the second phase with permittivity ϵ_2.

Solving Eq. (2) for ϵ^* in terms of complex permittivities ϵ_1, ϵ_2 and the volume fraction f of the first phase gives

$$\epsilon^*=\frac{1}{4}\left(\gamma+\sqrt{\gamma^2+8\epsilon_1\epsilon_2}\right),\quad \text{where } \gamma=(3f-1)\epsilon_1+(2-3f)\epsilon_2. \tag{3}$$

Here, γ can be expressed as a convex combination of permittivities ϵ_1 and ϵ_2 as: $\gamma = f(2\epsilon_1-\epsilon_2)+(1-f)(2\epsilon_2-\epsilon_1)$. The parameter γ in (3) can also be represented in a symmetric form as $\gamma=(3f_1-1)\epsilon_1+(3f_2-1)\epsilon_2$, where f_1 and f_2 are fractions of the components in the composite, which shows that the Bruggeman mixing formula is symmetric with respect to the interchanging the inclusion and matrix materials. We choose the positive sign of the square root in (3) because for real positive ϵ_1 and ϵ_2, the effective permittivity ϵ^* should lie between the values of ϵ_1 and ϵ_2.

When ϵ_2 goes to zero, the solution ϵ^* of Eq. (2) can have different behavior depending on the value of the volume fraction f of the phase 1. In this case the representation ϵ^* in (3) becomes $\epsilon^*=(\gamma+|\gamma|)/4$ where $\gamma=(3f-1)\epsilon_1$. The effective permittivity ϵ^* is zero if the volume fraction f is less than some threshold volume fraction f_c, and ϵ^* is strictly positive if the volume fraction f is bigger than the threshold value f_c:

$$\epsilon^*=\begin{cases}3\epsilon_1(f-f_c)/2 & \text{if } f_c<f<1,\\ 0 & \text{if } 0<f\leqslant f_c.\end{cases} \tag{4}$$

This critical volume fraction value f_c, $f_c=1/3$, is the critical filling factor or the percolation threshold for the phase 1.

The function $F(s)$ for the 3D Bruggeman effective permittivity model has the following form as a function of parameter $s=\epsilon_2/(\epsilon_2-\epsilon_1)$ on the complex s-plane:

$$\begin{aligned}F(s)&=1-\frac{\epsilon^*}{\epsilon_2}=1-\frac{\gamma}{4\epsilon_2}-\frac{1}{4}\sqrt{\left(\frac{\gamma}{\epsilon_2}\right)^2+8\frac{\epsilon_1}{\epsilon_2}}=\frac{3}{4}-\frac{1-3f}{4s}-\frac{1}{4}\sqrt{8\left(1-\frac{1}{s}\right)+\left(1-\frac{3f-1}{s}\right)^2}\\&=\frac{3}{4}-\frac{1-3f}{4s}-\frac{1}{4}\sqrt{\frac{9s^2-6(f+1)s+(3f-1)^2}{s^2}}.\end{aligned} \tag{5}$$

We can check that as expected, $F(s)\to 0$ as $s\to\infty$. We assume here that $\epsilon_2\neq 0$, otherwise we consider a symmetric analytic representation on a complex plane of variable $t=\epsilon_1/(\epsilon_1-\epsilon_2)$.

Theorem 1. *Let $\mu(x)$ represent the spectral measure function. The spectral function $F(s)$ in (5) has an analytic Stieltjes integral representation on the complex plane of variable s, $s=x+iy$:*

$$F(s)=\frac{A_0H(v)}{s}+\int_0^1\frac{\mathrm{d}\mu(x)}{s-x}=\frac{A_0H(v)}{s}+\int_0^1\frac{m(x)\mathrm{d}x}{s-x}, \tag{6}$$

where the function $H(v)$ is the Heaviside step function, the parameters v and A_0 are

$$v=f-f_c,\quad A_0=3v/2 \tag{7}$$

and the spectral density function $m(x)$ is

$$m(x)=\begin{cases}\frac{1}{4\pi x}\sqrt{-9x^2+6(f+1)x-(3f-1)^2} & \text{if } x_1<x<x_2,\\ 0 & \text{if } x\leqslant x_1 \text{ or } x\geqslant x_2,\end{cases} \tag{8}$$

where

$$x_{1,2}=\frac{f+1\pm\sqrt{8f(1-f)}}{3},\quad 0\leqslant x_1<x_2<1. \tag{9}$$

To prove Theorem 1, we first derive the spectral density formula (8) using Stieltjes inversion formula

$$m(x)=-\frac{1}{\pi}\lim_{y\to 0^+}\mathrm{Im}F(x+\mathrm{i}y). \tag{10}$$

In fact, for $s\neq 0$ and a fixed volume fraction f of one component in a two-phase composite ($0<f<1$), the quadratic inside the square root of (5) is zero at the points

$$x_{1,2}=\frac{f+1\pm\sqrt{8f(1-f)}}{3},\quad 0\leqslant x_1<x_2<1. \tag{11}$$

which can be verified using the quadratic formula. We see that for real values of s, the quadratic under the square root of (5) is negative for $x \in (x_1,x_2)$ and positive outside. In particular, we can define the square root (and hence the function $F(s)$) to be analytic on the whole complex plane, with only a finite cut removing the interval (x_1,x_2), and the point zero, from the domain of analyticity.

To ensure that $F(s) \to 0$ as $s \to \infty$, we have to choose the sign of the square root in (5) to be positive for real values for $s > x_2$. By analyticity, as we rotate 180 degrees from real $s > x_2$ to real $s < x_2$ through the upper half plane, the square root rotates through 90 degrees, giving a pure imaginary root, with positive imaginary part. Thus, by continuity we get

$$F(x+0^+\mathrm{i}) = \frac{3}{4} - \frac{1-3f}{4x} - \frac{\mathrm{i}}{4}\sqrt{\frac{|9x^2-6(f+1)x+(3f-1)^2|}{x^2}}, \quad \forall x \in (x_1,x_2). \tag{12}$$

Noting that only the square root term in (12) gives an imaginary part, we see immediately that

$$-\frac{1}{\pi}\lim_{y\to 0^+} \mathrm{Im}\ F(x+\mathrm{i}y) = \frac{1}{4\pi}\sqrt{\frac{|9x^2-6(f+1)x+(3f-1)^2|}{x^2}}, \quad \forall x \in (x_1,x_2). \tag{13}$$

Since the term in the absolute value is negative when $x \in (x_1,x_2)$, (13) can be simplified as

$$-\frac{1}{\pi}\lim_{y\to 0^+} \mathrm{Im}\ F(x+\mathrm{i}y) = \frac{1}{4\pi x}\sqrt{-9x^2+6(f+1)x-(3f-1)^2}, \quad \forall x \in (x_1,x_2). \tag{14}$$

On the other hand, for real values of x outside of (x_1,x_2), the square root in (5) is a real number, so that $F(x+0^+\mathrm{i})$ is real, its imaginary part is zero, and thus

$$-\frac{1}{\pi}\lim_{y\to 0^+} \mathrm{Im}\ F(x+\mathrm{i}y) = 0, \quad \forall x \notin (x_1,x_2). \tag{15}$$

From the Stietjes inversion formula (10), the limits (14) and (15) show that

$$m(x) = \begin{cases} \frac{1}{4\pi x}\sqrt{-9x^2+6(f+1)x-(3f-1)^2}, & x \in (x_1,x_2), \\ 0 & \text{otherwise}, \end{cases} \tag{16}$$

where x_1, x_2 are given in (9).

To complete the proof of Theorem 1, the following lemmas will be used to directly derive the Stieltjes integral representation formula (6).

Lemma 1. *For any complex number a with $|a| > 1$, the integral identity*

$$\int_{-1}^{1} \frac{\sqrt{1-w^2}}{w+a}\,\mathrm{d}w = (a-\sqrt{a^2-1})\pi \tag{17}$$

holds.

Proof. This is a standard integral identity on the real line, for real $a > 1$, as can be verified by Mathematica or a table of integrals. The integrand on the left is analytic in variable a and hence the parameterized integral can be extended to an analytic function on most of the complex plane, only excluding the real interval $[-1,1]$, which is the interval of integration.

Similarly, we extend the real root $\sqrt{a^2-1}$ to the complex-valued function $v(a) = \sqrt{a^2-1}$, choosing a branch cut so that it is continuous and analytic on most of the complex plane, only excluding the interval $[-1,1]$. We choose signs so that $\sqrt{a^2-1}$ is positive for real $a > 1$, and as a consequence of the choice of branch cut we will have $\sqrt{a^2-1}$ negative for real $a < -1$. In fact, we may note that

$$v(a) = a\sqrt{1-\frac{1}{a^2}} \quad \text{for all } |a| > 1, \tag{18}$$

where we use the usual power series expansion for the square root on the unit disk centered at 1.

Therefore, we have the signs correct and the two sides of Eq. (17) agree for $|a| > 1$ in the complex plane. By analyticity, they agree on the entire region on which they are analytic, namely the complex plane with the real interval $[-1,1]$ removed. This completes the proof of lemma. □

Lemma 2. *Let a and b be complex numbers, $a \neq b$, satisfying $|a| > 1$ and $|b| > 1$. The integral identity*

$$\int_{-1}^{1} \frac{\sqrt{1-w^2}}{(w+a)(w+b)}\,\mathrm{d}w = \frac{\pi}{b-a}\left(a-b+\sqrt{b^2-1}-\sqrt{a^2-1}\right) \tag{19}$$

holds.

Proof. For any complex numbers a, b with $a \neq b$, $|a| > 1$ and $|b| > 1$, a partial fraction expansion of the integrand on the left hand side of (19) shows that

$$\int_{-1}^{1} \frac{\sqrt{1-w^2}}{(w+a)(w+b)}\,dw = \frac{1}{b-a}\int_{-1}^{1} \frac{\sqrt{1-w^2}}{w+a}\,dw - \frac{1}{b-a}\int_{-1}^{1} \frac{\sqrt{1-w^2}}{w+b}\,dw$$
$$= \frac{\pi}{b-a}\left(a-\sqrt{a^2-1}\right) - \frac{\pi}{b-a}\left(b-\sqrt{b^2-1}\right) = \frac{\pi}{b-a}\left(a-b+\sqrt{b^2-1}-\sqrt{a^2-1}\right) \tag{20}$$

by Lemma 1. This completes the proof of lemma. □

Now we are ready to complete the proof of Theorem 1.

Proof of Theorem 1. The spectral density function $m(x)$ in (8) can be rewritten as

$$m(x) = \frac{1}{4\pi x}\sqrt{2-6(x-f)^2-3(x+f-1)^2}, \quad \text{for } x_1 < x < x_2, \tag{21}$$

where the values of x_1, x_2 are given in (9). We now intend to directly evaluate the integral

$$G(s) = \int_0^1 \frac{m(x)}{s-x}\,dx = \frac{1}{4\pi}\int_{x_1}^{x_2} \frac{\sqrt{2-6(x-f)^2-3(x+f-1)^2}}{x(s-x)}\,dx. \tag{22}$$

We introduce the variable $u = x-(1+f)/3$, in terms of which the function $G(s)$ can be rewritten as

$$G(s) = \frac{1}{4\pi}\int_{u_1}^{u_2} \frac{\sqrt{8f(1-f)-9u^2}}{(u+(1+f)/3)(s-u-(1+f)/3)}\,du, \tag{23}$$

where $u_1 = x_1-(1+f)/3$ and $u_2 = x_2-(1+f)/3$. Making a second change of variable with $w = 3u/\sqrt{8f(1-f)}$, we obtain

$$G(s) = \frac{-3}{4\pi}\int_{-1}^{1} \frac{\sqrt{1-w^2}}{\left(w+\frac{1+f}{\sqrt{8f(1-f)}}\right)\left(w+\frac{1+f}{\sqrt{8f(1-f)}}-\frac{3s}{\sqrt{8f(1-f)}}\right)}\,dw. \tag{24}$$

The integral on the right hand side of (24) has the same form of Eq. (19) as in Lemma 2, with

$$a = \frac{1+f}{\sqrt{8f(1-f)}} \quad \text{and} \quad b = \frac{1+f-3s}{\sqrt{8f(1-f)}} \quad \text{for } 0 < f < 1. \tag{25}$$

Note that a is real, and greater than 1, since $(1+f) \geqslant \sqrt{8f(1-f)}$, and b can be assumed large by suitable choice of the complex variable s. Analytic continuation will imply agreement between $F(s)$ and the integral representation (6) for all s in the domain of analyticity. Hence we can apply Lemma 2 and solve for $G(s)$ as

$$G(s) = \frac{-3}{4\pi}\frac{\pi}{b-a}\left(a-b+\sqrt{b^2-1}-\sqrt{a^2-1}\right)$$
$$= \frac{-3}{4}\frac{\sqrt{8f(1-f)}}{-3s}\left(\frac{3s}{\sqrt{8f(1-f)}}+\sqrt{\frac{(1+f-3s)^2}{8f(1-f)}-1}-\sqrt{\frac{(1+f)^2}{8f(1-f)}-1}\right)$$
$$= \frac{3}{4}+\frac{1}{4s}\left(\sqrt{(1+f-3s)^2-8f(1-f)}-\sqrt{(1+f)^2-8f(1-f)}\right)$$
$$= \frac{3}{4}+\frac{1}{4s}\left(\sqrt{9s^2-6(1+f)s+(1-3f)^2}-\sqrt{(1-3f)^2}\right) = \frac{3}{4}-\frac{|1-3f|}{4s}+\frac{1}{4s}\sqrt{9s^2-6(1+f)s+(1-3f)^2}. \tag{26}$$

In order to move the variable s into the square root in the last term on the right hand side of (26), we rewrite this term by denoting the complex variable $s = |s|\arg(s)$ with $n = 0, 1$ as in the following

$$\frac{1}{4s}\sqrt{s^2\left(9-\frac{6(1+f)}{s}+\frac{(1-3f)^2}{s^2}\right)} = \frac{1}{4s}|s|e^{(\arg(s)i+n\pi)}\sqrt{\left(9-\frac{6(1+f)}{s}+\frac{(1-3f)^2}{s^2}\right)}. \tag{27}$$

Since $\lim_{s\to\infty} G(s) = 0$ in (22), we must choose the branch cut with $n = 1$ on the right hand side of (27), so that

$$G(s) = \frac{3}{4}-\frac{|1-3f|}{4s}-\frac{1}{4}\sqrt{9-\frac{6(1+f)}{s}+\frac{(1-3f)^2}{s^2}} = \frac{3}{4}-\frac{|1-3f|}{4s}-\frac{1}{4}\sqrt{\frac{9s^2-6(f+1)s+(3f-1)^2}{s^2}}. \tag{28}$$

It should be noted that

$$(1-3f) = |1-3f| + 2(1-3f)H(3f-1), \tag{29}$$

where H is the Heaviside step function. The function $F(s)$ in (5) can be calculated directly in terms of $G(s)$ in (28) as

$$F(s) = \frac{3f-1}{2s} H(f-1/3) + G(s). \tag{30}$$

Therefore, we obtain the Stieltjes integral representation

$$F(s) = \frac{3f-1}{2s} H(f-f_c) + \int_{x_1}^{x_2} \frac{m(x)\,\mathrm{d}x}{s-x} = \frac{A_0 H(v)}{s} + \int_0^1 \frac{m(x)\,\mathrm{d}x}{s-x}. \tag{31}$$

Here the parameters v and A_0 are given by

$$v = f - f_c, \quad A_0 = 3v/2, \quad f_c = 1/3. \tag{32}$$

Next we will examine the pole at $s = 0$ for the Stieltjes integral representation of $F(s)$ in (31). For a small s, from (5) and (26), we have

$$F(s) \approx -\frac{1-3f}{4s} - \frac{1}{4}\sqrt{\frac{(3f-1)^2}{s^2}} = \frac{(3f-1)+|3f-1|}{4s}, \tag{33}$$

which is zero when $(3f-1)$ is negative (i.e. $F(s)$ has no pole at $s = 0$ in this case), and is just $(3f-1)/2s$ when $(3f-1)$ is positive. Thus, in the case where $f \leqslant f_c = 1/3$, the Stieltjes integral representation

$$F(s) = \int_{x_1}^{x_2} \frac{m(x)\,\mathrm{d}x}{s-x} \tag{34}$$

holds because $F(s)$ has no pole at the origin. In the case where $f > f_c = 1/3$, from (33), we have to insert a pole at $s = 0$ with residue $(3f-1)/2$ and obtain

$$F(s) = \frac{3f-1}{2s} + \int_0^1 \frac{m(x)}{s-x}\,\mathrm{d}x, \tag{35}$$

which agrees with the integral representation (31). Therefore, from (31), (34) and (35), we conclude that

$$F(s) = \begin{cases} \dfrac{A_0}{s} + \displaystyle\int_0^1 \frac{m(x)\mathrm{d}x}{s-x} & \text{if } f_c < f < 1, \\ \displaystyle\int_0^1 \frac{m(x)\mathrm{d}x}{s-x} & \text{if } 0 < f \leqslant f_c, \end{cases} \tag{36}$$

where $A_0 = (3f-1)/2$, $m(x)$ is given in (8) and (9). This completes the proof of theorem. □

Remark 1. An alternative proof of Theorem 1 based on the Stieltjes inversion formula (10) is given in Appendix A.

The spectral density function $m(x)$ satisfies the sum rule:

$$\int_{x_1}^{x_2} m(x)\mathrm{d}x = \int_{x_1}^{x_2} \mathrm{d}\mu(x) = f. \tag{37}$$

The sum rule property (37) gives the zero moment μ_0 of the spectral measure μ which can be used to calculate the volume fraction f of one of the constituents from known effective complex permittivity of the composite.

3. Rational (Padé) approximation

In this section we discuss Padé approximation of the spectral function which allows us to construct accurate approximation to the continuous spectral density in the Bruggeman effective medium model using a small number of poles. Based on the theory of reconstruction of the spectral measure from known effective permittivity developed in [10] and the approach to reconstruction of the spectral measure using rational function approximation in [38,39], the spectral function $\mu(x)$ in (6) can be approximated by a step function with a finite number of steps, so that the spectral density function $m(x)$ in (6) has the form:

$$m(x) \simeq \hat{m}(x) = \sum_{n=1}^{q} A_n \delta(x - s_n), \quad x \in [0,1), \tag{38}$$

where $\delta(x)$ is the Dirac delta function. It was shown in [39], that the spectral properties of the related operator impose constraints on the amplitudes A_n and location of the poles $s_1, s_2, \ldots, s_q$ of the delta functions in this sum: $0 \leqslant A_n < 1$, $0 \leqslant s_1 < s_2 < \cdots < s_q < 1$. In this case, the function $\mu(x)$ satisfying (6) can be approximated by

$$\mu(x) = \int_0^{x^+} \mathrm{d}\mu(t) \simeq \int_0^{x^+} \mathrm{d}\hat{\mu}(t) = \sum_{n=1}^{q} A_n \int_0^{x^+} \delta(t - s_n)\mathrm{d}t, \tag{39}$$

so that

$$\mu(x) \simeq \hat{\mu}(x) = \sum_{n=1}^{q} A_n H(x - s_n), \quad x \in [0,1), \tag{40}$$

where $H(x)$ is the Heaviside step function. The function $\mu(x)$ defined for $x \in [0,1)$ is a non-decreasing, non-negative function corresponding to the Stieltjes function $F(s)$. Thus, the approximation $\widehat{F}(s)$ of the function $F(s)$ is given by

$$F(s) \simeq \widehat{F}(s) = \sum_{n=1}^{q} \frac{A_n}{s - s_n} \tag{41}$$

with constraints

$$0 \leqslant s_n < 1, \quad 0 \leqslant A_n < 1, \quad 0 < \sum A_n < 1. \tag{42}$$

Here s_n is the n-th simple pole on the unit interval with positive residue A_n, q is the total number of poles. Note that the effective permittivity of a composite material could be frequency dependent; it follows from (41) that the approximation of the frequency-dependent effective permittivity ϵ^* is given by

$$\epsilon^*(\omega) = \epsilon_2(\omega)[1 - F(s)] \simeq \epsilon_2(\omega)\left[1 - \sum_{n=1}^{q} \frac{A_n}{s - s_n}\right], \quad s = \frac{\epsilon_2(\omega)}{\epsilon_2(\omega) - \epsilon_1(\omega)}. \tag{43}$$

The real parameters A_n and s_n in the representation (43) depend purely on the microgeometry of the composite.

The right hand side of (41) can be viewed as rational function approximation:

$$\widehat{F}(s) = \sum_{n} \frac{A_n}{s - s_n} = \frac{\phi(s)}{\psi(s)}, \tag{44}$$

where the degree of the polynomial $\phi(s)$ is lower than the degree of the polynomial $\psi(s)$. Let p and q be the orders of polynomials $\phi(s)$ and $\psi(s)$ with $p \leqslant q$, respectively. The rational $[p,q]$-Padé approximation of $F(s)$ can be written as (see [1])

$$\widehat{F}(s) = F_{[p,q]}(s) = \frac{\phi(s)}{\psi(s)} = \frac{a_0 + a_1 s + a_2 s^2 + \cdots + a_p s^p}{b_0 + b_1 s + b_2 s^2 + \cdots + b_q s^q}, \tag{45}$$

where a_l ($l = 0,1,\ldots,p$) and b_k ($k = 0,1,\ldots,q$) are the coefficients of real polynomials $\phi(s)$ and $\psi(s)$, respectively. Since (38) provides an approximation to a function in the unit interval, all the zeroes of the denominator $\psi(s)$ should be simple and all poles s_n of the function $F(s)$ lie in the interval $[0,1)$. We normalize the polynomial coefficient $b_1 = 1$ in the denominator $\psi(s)$; this allows us to model the physically realizable zero pole of $F(s)$.

We further assume that the measurements $\epsilon^*(\omega_j)$ of the effective permittivity ϵ^* are available at sample frequencies ω_j ($j = 1,2,\ldots,N$). The measured data pairs $(\omega_j, \epsilon^*(\omega_j))$ can be transformed to data pairs (z_j, f_j) in the complex s-plane:

$$f_j = 1 - \frac{\epsilon^*(\omega_j)}{\epsilon_2(\omega_j)}, \quad z_j = \frac{\epsilon_2(\omega_j)}{\epsilon_2(\omega_j) - \epsilon_1(\omega_j)}, \quad (j = 1,2,\ldots,N). \tag{46}$$

Here f_j is the measured value of the function $F(s)$ at the sample point z_j, $f_j = F(z_j)$ with N being the total number of data points.

To formulate the optimization problem for the coefficients a_l's and b_k's in (45), we require that the constructed approximation $\widehat{F}(s)$ agreed with the measured values of $F(s)$ at the points z_j. Then Eq. (45) can be written as

$$\frac{\phi(z_j)}{\psi(z_j)} = \frac{a_0 + a_1 z_j + a_2 z_j^2 + \cdots + a_p z_j^p}{b_0 + z_j + b_2 z_j^2 + \cdots + b_q z_j^q} = f_j, \tag{47}$$

where a_l ($l = 0,\ldots,p$), b_k ($k = 0,\ldots,q, k \neq 1$) are required unknown coefficients. Eq. (47) is equivalent to following system

$$a_0 + a_1 z_j + \cdots + a_p z_j^p - b_0 f_j - b_2 f_j z_j^2 - \cdots - b_q f_j z_j^q = f_j z_j, \quad (j = 1,2,\ldots,N). \tag{48}$$

Therefore, the system (48) for the unknown real coefficients a_l's and b_k's of the rational approximation $\phi(s)/\psi(s)$ can be further expressed as the following system

$$\mathbf{Sc} = \mathbf{d}, \tag{49}$$

where

$$\mathbf{S} = \begin{pmatrix} 1 & z_1 & z_1^2 & \ldots & z_1^p & -f_1 & -f_1 z_1^2 & -f_1 z_1^3 & \ldots & -f_1 z_1^q \\ 1 & z_2 & z_2^2 & \ldots & z_2^p & -f_2 & -f_2 z_2^2 & -f_2 z_2^3 & \ldots & -f_2 z_2^q \\ \ldots & \ldots & \ldots & \ldots & \ldots & \ldots & \ldots & \ldots & \ldots & \ldots \\ 1 & z_N & z_N^2 & \ldots & z_N^p & -f_N & -f_N z_N^2 & -f_N z_N^3 & \ldots & -f_N z_N^q \end{pmatrix}.$$

$$\mathbf{c} = [a_0, a_1, \ldots, a_p, b_0, b_2, b_3, \ldots, b_q]^\top, \mathbf{d} = [f_1 z_1, f_2 z_2, \ldots, f_N z_N]^\top \tag{50}$$

and the symbol $[\,\cdot\,]^\top$ indicates a transposed matrix. It is clear that in order for the Padé coefficients a_l's and b_k's to be uniquely determined, the total number of the measurements must be greater or equal to the number of coefficients, i.e., $N > p + q + 1$. The reconstruction problem of determining the column vector $\mathbf{c} = [a_0, a_1, \ldots, a_p, b_0, b_2, \ldots, b_q]^\top$ of real coefficients in (49), (50) is an inverse problem. It is ill-posed and requires regularization to develop a stable numerical algorithm. In the present work we solve a constrained minimization problem described below with constraints given in (42).

Let complex matrix $\mathbf{S}$ be $\mathbf{S} = \mathbf{S}_\mathrm{R} + \mathrm{i}\mathbf{S}_\mathrm{I}$ and the vector of data points $\mathbf{d}$ be $\mathbf{d} = \mathbf{d}_\mathrm{R} + \mathrm{i}\mathbf{d}_\mathrm{I}$ where subindices R and I stand for the real and imaginary parts. To construct a real solution vector $\mathbf{c}$ of $[p, q]$-Padé coefficients for the problem (49), (50), we introduce a minimization functional $\mathscr{T}^\lambda(\mathbf{c}, \mathbf{d}_\mathrm{R}, \mathbf{d}_\mathrm{I})$ with a penalization term which constrains the set of minimizers. The inequalities (42) for the residues and poles of the function $F(s)$ are used to impose constraints for the set of minimizers of the problem. We reformulate the problem as a constrained minimization using Tikhonov regularization [33] with the regularization parameter λ $(0 < \lambda < 1)$ to be chosen properly:

$$\begin{aligned} &\min_{\mathbf{c}} \mathscr{T}^\lambda(\mathbf{c}, \mathbf{d}_\mathrm{R}, \mathbf{d}_\mathrm{I}) = \min_{\mathbf{c}} \{\|\mathbf{S}_\mathrm{R}\mathbf{c} - \mathbf{d}_\mathrm{R}\|^2 + \|\mathbf{S}_\mathrm{I}\mathbf{c} - \mathbf{d}_\mathrm{I}\|^2 + \lambda^2\|\mathbf{c}\|^2\} \\ &\text{s.t. } 0 \leqslant A_n < 1,\ 0 \leqslant s_n < 1,\ 0 < \sum A_n < 1, \quad n = 1, 2, \ldots, q. \end{aligned} \tag{51}$$

Here $\|\cdot\|$ denotes the usual Euclidean norm and parameters s_n, A_n are poles and residues of the partial fractions decomposition (41) of the reconstructed $[p,q]$-Padé approximation of the spectral function. To find the minimizer of the problem, we solve the corresponding Euler equation; its solution is given by

$$\mathbf{c} = \left\{\mathbf{S}_\mathrm{R}^\top\mathbf{S}_\mathrm{R} + \mathbf{S}_\mathrm{I}^\top\mathbf{S}_\mathrm{I} + \lambda\mathbf{I}_{p+q+1}\right\}^{-1}\left\{\mathbf{S}_\mathrm{R}^\top\mathbf{d}_\mathrm{R} + \mathbf{S}_\mathrm{I}^\top\mathbf{d}_\mathrm{I}\right\}. \tag{52}$$

Here $\mathbf{I}_{p+q+1}$ denotes the $(p + q + 1) \times (p + q + 1)$ identity matrix. After reconstruction of the vector $\mathbf{c}$ of the coefficients of rational function approximation of $\widehat{F}(s)$, its decomposition into partial fractions (41), gives $[p,q]$-Padé approximation of the spectral function $F(s)$.

In the next section, we show results of numerical simulations and application of the technique to the problem of estimation of volume fractions of constituents in the mixture, which is a particular case of the problem of extraction of information about structural parameters of composites. Indeed, it was shown in [5] for a case of discrete spectral density function in analytical representation, that the volume fraction f of subdomains occupied by the first material in composite is a sum of all residues in the analytical integral representation:

$$\sum A_n = f. \tag{53}$$

The reconstructed Padé approximation, function $\widehat{F}(s)$, can be used to calculate the volume fraction of the first material in the composite using formula (53) which gives an approximation to the sum rule (37).

4. Numerical examples

This section describes numerical experiments using the inversion technique in Section 3 applied to the problem of reconstruction of the spectral density of the 3D Bruggeman EMA model derived in Section 2. To demonstrate the effectiveness of the method, we apply it to the problem of recovering the volume fractions of the constituents from the effective permittivity of the Bruggeman composite.

3D Bruggeman EMA model was used to simulate the effective complex permittivity of the two-phase composite material for a range of frequencies, then these simulated values were taken as data for the rational approximation algorithm which reconstructs poles and residues of the approximation $\widehat{F}(s)$. The approximation $\hat{m}(x)$ of the spectral density function $m(x)$ at each location of the reconstructed poles s_n with corresponding residues A_n is calculated using the following formula

$$\frac{\mathrm{d}\mu(s_n)}{\mathrm{d}x} = m(s_n) \approx \hat{m}(s_n) = \frac{A_n}{(s_{n+1} - s_{n-1})/2}, \quad (n = 1, 2, \ldots, q_0) \tag{54}$$

where $s_0 = x_1, s_{q_0+1} = x_2$, the values of x_1, x_2 are given in (9), and q_0 is the total number of the validly reconstructed poles of spectral function.

We model a frequency-dependent metallic particles composite of magnesium and magnesium fluoride ($\mathrm{MgMgF_2}$) using the described 3D Bruggeman EMA model. The frequency-dependent permittivity of the metallic particles of magnesium (Mg) taken as inclusion material in the composite, is given by the Drude dielectric model (see [20]):

$$\epsilon_1 = \epsilon_\mathrm{metal}(\omega) = 1 - \frac{\omega_\mathrm{p}^2}{\omega(\omega + \mathrm{i}\tau^{-1})}. \tag{55}$$

Here ω is the circular frequency, ω_p is the plasma frequency, τ is the relaxation time and $\mathrm{i} = \sqrt{-1}$. The parameter ω_p and the relaxation time τ of the dielectric metallic grains of magnesium (Mg) are given in Table 1. The permittivity of magnesium fluoride ($\mathrm{MgF_2}$) considered as the background matrix material in the mixture, is taken as a dispersionless constant, $\epsilon_2 = 1.96$, it is shown in Table 1 as well. The frequency-dependent values of the effective complex permittivity ϵ^* for the

Table 1
Physical parameters of complex permittivity of $MgMgF_2$ composite.

Material	τ	ω_p	Material	Permittivity ϵ_2
Mg	2.5×10^{-16} s	9.4×10^{15} s^{-1}	MgF_2	1.96

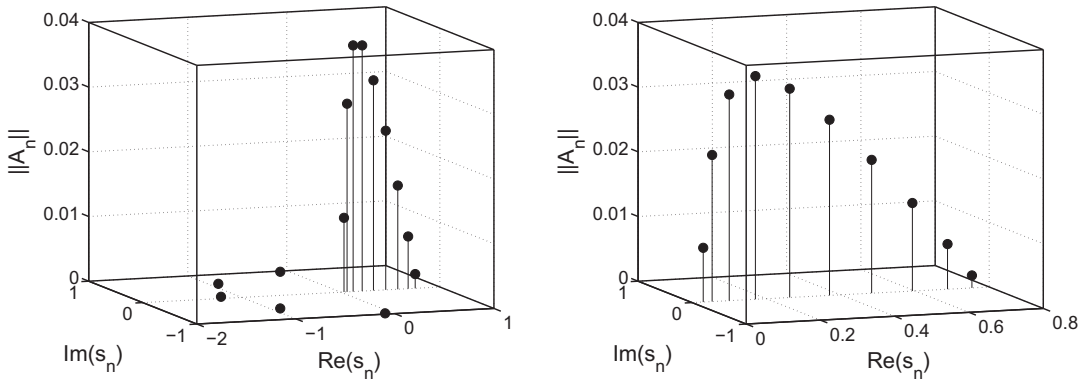

Fig. 1. Poles and residues of the spectral function recovered without constraints for 20%Mg-80%MgF_2 mixture with $p = q = 14$ (left) and $p = q = 10$ (right).

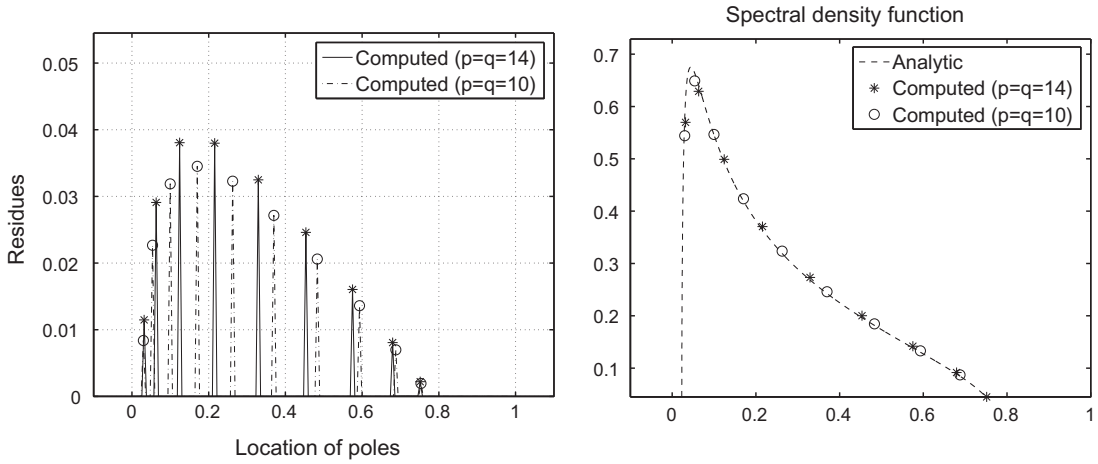

Fig. 2. Valid poles and residues of the spectral function (left) and the spectral density function $m(x)$ (right) recovered with constraints for 20%Mg-80%MgF_2 mixture ($p = q = 14$ and $p = q = 10$).

mixture of $MgMgF_2$ with magnesium (Mg) inclusions were simulated in a range of frequency: $0 \leqslant \omega \leqslant \omega_p = 9.4 \times 10^{15}$ s^{-1} using described model of microstructure of composite materials. Two cases of the composites of magnesium and magnesium fluoride ($MgMgF_2$) with low volume fraction and large volume fraction of the magnesium (Mg) inclusion phase are tested in the numerical experiments.

4.1. Results for low volume fraction f (0 < f ⩽ 1/3)

The recovered poles and residues of the spectral function for 3D Bruggeman EMA model with volume fraction $f = 0.20$ of magnesium (Mg) component are shown in the left part of Fig. 1 for the case $p = q = 14$ and in the right part of Fig. 1 for the case $p = q = 10$. Shown are results of inversion without constraints in the inversion procedure when no noise was added to the data. It can be seen from the left part of Fig. 1 that there are 9 validly reconstructed poles which are located between 0.023 and 0.777 in the unit interval $[0,1)$ and the other 5 poles located off the unit interval in the complex s-plane. The left part of Fig. 2 illustrates the recovery of valid poles and residues of the spectral function for 3D Bruggeman EMA model for the case with constraints in the inversion process. The volume fraction of the magnesium (Mg) component is calculated by the sum of residues corresponding to validly reconstructed poles using formula (53) as $f = \sum A_n \approx 0.1999986623$ with $q_0 = 9$ for the case when $p = q = 14$ and $f = \sum A_n \approx 0.2000000075$ with $q_0 = 10$ when $p = q = 10$, respectively. We compared analytically and numerically calculated spectral density functions. The right part of Fig. 2 shows the true and computed spectral density functions calculated using formula (54). The true and computed real and imaginary parts of $F(s)$ at 30 data points are

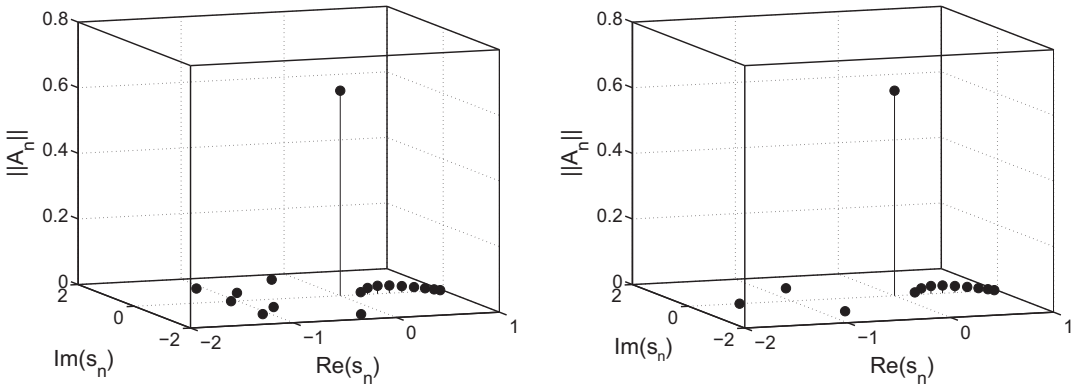

Fig. 3. 3D Bruggeman EMA model of 75%Mg-25%MgF_2 composite. Poles and residues reconstructed without constraints, Padé approximations of order $p = q = 17$ (left) and $p = q = 13$ (right).

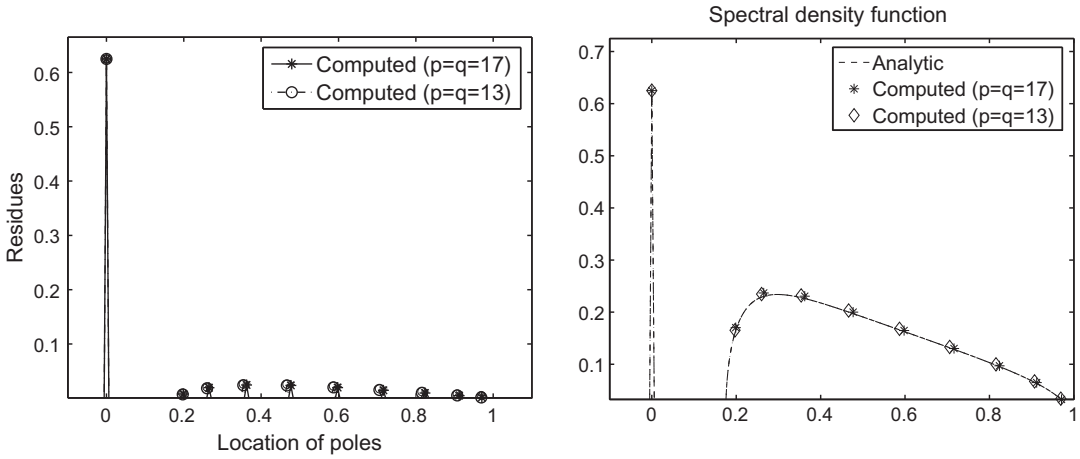

Fig. 4. Reconstructed with constraints poles and residues (left) and spectral density function $m(x)$ (right) for 3D Bruggeman EMA model of 75%Mg-25%MgF_2 mixture ($p = q = 17$ and $p = q = 13$).

demonstrated in left part of Fig. 5. The imaginary part of the spectral function $F(s)$ is a non-positive function in the complex s-plane.

4.2. Results for large volume fraction f (1/3 < f < 1)

For large volume fraction of the magnesium inclusion phase in the mixture of magnesium and magnesium fluoride ($MgMgF_2$), the spectral function exhibits different behavior compared with the case of low volume fraction of inclusion component. There is an additional isolated pole of the spectral function which corresponds to the delta function of the spectral density function at the origin. Fig. 3 shows the recovered poles and residues of the spectral function without constraints in the inversion process for different orders $p = q = 17$ (left) and $p = q = 13$ (right) for 75%Mg–25%MgF_2 mixture when there is no noise in the data. The additional isolated pole with amplitude $A_0 = 0.625$ is located at $s = 0$. There are other 9 validly reconstructed poles of small amplitudes lying in the unit interval between 0.175 and 0.992 shown in the left part of Fig. 4. The right part of Fig. 4 shows the analytical spectral density function and the one numerically reconstructed using Padé approximation of orders $p = q = 17$ and $p = q = 13$. The volume fraction of the magnesium (Mg) inclusion phase is estimated fairly well using formula (53) calculated as $f = \sum A_n \simeq 0.749999773$ for $p = q = 17$ and $f = \sum A_n \simeq 0.749999952$ for $p = q = 13$. The true effective permittivity ϵ^* used at 40 data points and computed effective permittivity are illustrated in the right part of Fig. 5.

4.3. Sensitivity analysis

The purpose of the next series of computations is to numerically examine the stability of the calculated volume fractions of magnesium (Mg) component in the mixture of magnesium and magnesium fluoride ($MgMgF_2$) for the 3D Bruggeman effective medium model. To simulate the noisy data, we used a uniformly distributed random noise calculated as percentage of the true value of effective permittivity ϵ^* at each measured point of 40 sample data in the same range of frequency as

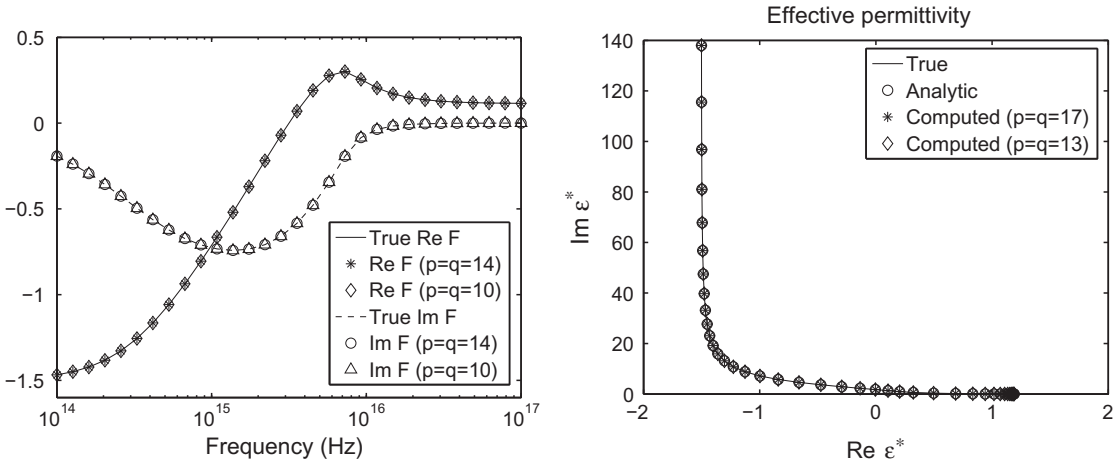

Fig. 5. Left: True and computed real and imaginary parts of $F(s)$ for 3D Bruggeman EMA model of 20%Mg-80%MgF_2 mixture ($p = q = 14$ and $p = q = 10$). Right: True and computed real and imaginary parts of ϵ^* for 3D Bruggeman EMA model of 75%Mg-25%MgF_2 composite ($p = q = 17$ and $p = q = 13$).

Table 2
Volume fractions calculated for the 3D Bruggeman EMA model using Padé approximation of order $p = q = 7$ at 40 sample data points with added noise levels of 1%, 3%, 5%.

Noise (%)	$f = 0.05$	$f = 0.15$	$f = 0.25$	$f = 0.35$	$f = 0.45$	$f = 0.55$	$f = 0.65$	$f = 0.75$
1	0.050097	0.149548	0.250053	0.349527	0.449391	0.550156	0.649809	0.750267
3	0.050317	0.148717	0.251254	0.350853	0.450891	0.550832	0.653160	0.749347
5	0.051151	0.147860	0.252113	0.351477	0.452154	0.551624	0.655060	0.745581

described in this section. This sensitivity test was done with a Padé approximation of order $p = q = 7$. A summary of the sensitivity analysis for the calculated volume fractions of magnesium component for $MgMgF_2$ composites of various volume fractions of magnesium inclusion phase using data with 1%, 3%, 5% noise is shown in Table 2. The first row in the table shows the true volume fractions of Mg component and the other three rows present the calculated volume fractions of the Mg phase. The results of computations show that even with added noise, the recovered volume fractions of magnesium component agree with the true values. This demonstrates the stability of the reconstruction algorithm.

5. Conclusion

In this paper, we have presented the derivation of an analytic Stieltjes integral representation for the 3D Bruggeman effective medium model which has continuous spectral density function. The spectral function containing important information about the microgeometry of the medium can be used to find the effective behavior of heterogeneous material, it also can be used to infer information about the composite's structure. We used constrained rational Padé algorithm [39] to construct a low order discrete approximation of the continuous spectral density function, such approximation consists of small number of poles. Using derived Stieltjes integral representation, we investigated efficiency of the constrained Padé approximation method for inverse homogenization for the case of Bruggeman composite model with continuous spectral density. The performed numerical experiments for estimation of the fractions of components in a mixture of magnesium and magnesium fluoride demonstrate the effectiveness of the algorithm.

Acknowledgments

This work was supported by NSF Grants DMS-0508901 and DMS/CMG-0934721. We gratefully acknowledge generous support from NSERC, MITACS, PIMS, and sponsors of the POTSI and CREWES projects. The first author is also funded by a Postdoctoral Fellowship at the University of Calgary.

Appendix A. An alternative proof of Theorem 1 based on Stieltjes inversion formula

Here we first intend to show that the spectral density function $m(x)$ in (8) is equivalently given by

$$m(x) = \begin{cases} \frac{1}{4\pi x}\sqrt{8f(1-f) - (3x-1-f)^2} & \text{if } x_1 < x < x_2, \\ 0 & \text{if } x \leqslant x_1 \text{ or } x \geqslant x_2, \end{cases} \tag{A.1}$$

where

$$x_{1,2} = \frac{1}{9}\left[4 + 3v \mp 2\sqrt{(1+3v)(4-6v)}\right], \quad 0 \leqslant x_1 < x_2 < 1. \tag{A.2}$$

In fact, for $s = x + \mathrm{i}y$, the complex spectral function $F(s)$ in (5) can be written explicitly in terms of x and y as

$$F(x+\mathrm{i}y) = \frac{3}{4} - \frac{(1-3f)x}{4(x^2+y^2)} - \mathrm{i}\frac{(3f-1)y}{4(x^2+y^2)} - \frac{1}{4}\sqrt{g_3 + \mathrm{i}g_4}, \tag{A.3}$$

where

$$g_3 = \frac{(x^2+y^2-(3f-1)x)^2 - y^2(3f-1)^2}{(x^2+y^2)^2} - 8g_1, \tag{A.4}$$

$$g_4 = \frac{2y(3f-1)(x^2+y^2-(3f-1)x)}{(x^2+y^2)^2} + 8yg_2 \tag{A.5}$$

and

$$g_1 = \frac{x}{x^2+y^2} - 1, \quad g_2 = \frac{1}{x^2+y^2}, \quad 1 - \frac{1}{s} = -g_1 + \mathrm{i}yg_2. \tag{A.6}$$

Let w denote expression under the square root in (A.3), $w = g_3 + \mathrm{i}g_4 = |g_3 + \mathrm{i}g_4|\mathrm{e}^{\mathrm{i}\theta}$, where $\theta = \arg(w) \in [0, 2\pi)$, so that

$$\cos\theta = \frac{g_3}{\sqrt{g_3^2+g_4^2}}, \quad \sin\theta = \frac{g_4}{\sqrt{g_3^2+g_4^2}}. \tag{A.7}$$

Thus, the imaginary part of the square root term in (A.3) can be expressed as

$$\mathrm{Im}\sqrt{g_3 + \mathrm{i}g_4} = \sqrt[4]{g_3^2+g_4^2}\,\sin\left(\frac{\theta + 2k\pi}{2}\right), \quad k = 0, 1. \tag{A.8}$$

In the following analysis, it should be noted that the spectral density function $m(x)$ is a real and non-negative function which is defined in the unit interval $x \in [0,1]$ by the Stieltjes inversion formula (10). In order to obtain the non-negative real-valued function $m(x)$ in the unit interval, the imaginary part of the square root term in (A.3) should be positive so that we must choose the positive sine function in (A.8). This requires $k = 0$ due to the fact that function $\sin(\pi + \theta/2) < 0$ when $k = 1$ in (A.8). Thus, from (A.8), the imaginary part of the complex function $F(x + \mathrm{i}y)$ in (A.3) must have the following form

$$\mathrm{Im}F(x+\mathrm{i}y) = -\frac{(3f-1)y}{4(x^2+y^2)} - \frac{1}{4}\sqrt[4]{g_3^2+g_4^2}\,\sin\frac{\theta}{2}, \tag{A.9}$$

where g_3 and g_4 are given in (A.4) and (A.5), respectively.

Case I: $x \in (0,1]$ and volume fraction $f \in (0,1)$. For a fixed $x \neq 0$, taking limit as y goes to 0^+ for the functions g_1, g_2, g_3 and g_4 in (A.4)–(A.6), we obtain

$$\lim_{y\to 0^+} g_1 = \frac{1}{x} - 1, \quad \lim_{y\to 0^+} g_2 = \frac{1}{x^2}, \quad \lim_{y\to 0^+} g_4 = 0 \tag{A.10}$$

and

$$\lim_{y\to 0^+} g_3 = \frac{1}{x^2}[(3x-(1+f))^2 - 8f(1-f)]. \tag{A.11}$$

The right hand side function in Eq. (A.11) is a concave upward quadratic polynomial in x which has two different roots in the unit interval:

$$x_{1,2} = \frac{1}{9}\left[4 + 3v \mp 2\sqrt{(1+3v)(4-6v)}\right], \quad 0 \leqslant x_1 < x_2 < 1, \tag{A.12}$$

where $v = f - f_c$, so that

$$\lim_{y\to 0^+} g_3 < 0 \quad \text{where } x_1 < x < x_2 \tag{A.13}$$

and

$$\lim_{y\to 0^+} g_3 > 0 \quad \text{where } x < x_1 \text{ or } x > x_2. \tag{A.14}$$

We consider separately the two cases given in (A.13) and (A.14). It is seen from (A.13) that for $x \in (x_1, x_2)$, the function $g_3(x,y) < 0$ for sufficiently small positive values of y. Hence, the angle θ of the complex number w must be restricted to the interval $\theta \in (\pi/2, 3\pi/2)$. Thus, from the fact that

$$\lim_{y\to 0^+}\cos\theta=-1,\quad \lim_{y\to 0^+}\sin\theta=0, \tag{A.15}$$

we get

$$\lim_{y\to 0^+}\theta=\pi. \tag{A.16}$$

Therefore, taking the limit in (A.9) as y goes to 0^+, it follows from (A.16) that

$$\lim_{y\to 0^+}\mathrm{Im}F(x+\mathrm{i}y)=-\frac{1}{4}\lim_{y\to 0^+}\sqrt[4]{g_3^2+g_4^2}\sin\left(\frac{\theta}{2}\right)=-\frac{1}{4}\lim_{y\to 0^+}\sqrt{|g_3|}. \tag{A.17}$$

By substituting (A.17) into (10), the spectral density function $m(x)$ is obtained as

$$m(x)=\frac{1}{4\pi x}\sqrt{8f(1-f)-(3x-1-f)^2}\quad \text{if } x_1<x<x_2. \tag{A.18}$$

For the second case $x<x_1$ and $x>x_2$, (A.14) gives that $g_3(x,y)>0$ for sufficiently small positive values of y, so that the angle θ of the complex number w must be in the interval $\theta\in(0,\pi/2)\bigcup(3\pi/2,2\pi)$. Thus,

$$\lim_{y\to 0^+}\cos\theta=1,\quad \lim_{y\to 0^+}\sin\theta=0 \tag{A.19}$$

and we obtain

$$\lim_{y\to 0^+}\theta=2l\pi,\quad l=0,1. \tag{A.20}$$

By substituting (A.20) into (10) and (A.17), we obtain for $x<x_1$ and $x>x_2$ ($l=0,1$):

$$m(x)=\frac{1}{4\pi}\lim_{y\to 0^+}\mathrm{Im}\sqrt{g_3+\mathrm{i}g_4}=\frac{1}{4\pi}\lim_{y\to 0^+}\sqrt{|g_3|}\sin(l\pi)=0. \tag{A.21}$$

From (A.18) and (A.21), we conclude that (A.1) holds where x_1 and x_2 are given in (A.12).

It should be noted that when volume fraction $f=f_c=1/3$, the spectral density function in (A.1) has the following simple form

$$m(x)=\begin{cases}\frac{1}{4\pi x}\sqrt{x(8-9x)} & \text{if } 0<x<\frac{8}{9},\\ 0 & \text{if } \frac{8}{9}\leqslant x\leqslant 1.\end{cases} \tag{A.22}$$

(A.22) gives a maximal subinterval $(0,8/9)\subset[0,1]$ in which the function $m(x)$ is positive.

Next, we consider asymptotic behavior of the imaginary part of the spectral function $F(s)$, i.e., $\mathrm{Im}F(x+\mathrm{i}y)$ when $x\to 0$, to analyze the behavior of the function $m(x)$ at the origin. For sufficiently small positive x (i.e., $x\approx 0$),we introduce polar coordinates $x=r\cos\phi$, $y=r\sin\phi$ in the first quadrant where $r>0$ and $\pi/4<\phi\leqslant\pi/2$. The real and imaginary parts for the complex number $w=g_3+\mathrm{i}g_4=|g_3+\mathrm{i}g_4|\mathrm{e}^{\mathrm{i}\theta}$ in (A.4), (A.5) where $\theta\in[0,2\pi)$ can be represented as

$$g_3=[9r^2-6r(1+f)\cos\phi+(3f-1)^2\cos(2\phi)]/r^2, \tag{A.23}$$

$$g_4=[(8+2(3f-1))r\sin\phi-(3f-1)^2\sin(2\phi)]/r^2. \tag{A.24}$$

Case II: $x\approx 0$ and volume fraction $f\neq 1/3$. In this case, for sufficiently small r, it is seen from (A.23), (A.24) that we must have $\theta\in(\pi/2,3\pi/2)$ because $g_3<0$, and we also have

$$\lim_{r\to 0}\tan\theta=\lim_{r\to 0}\frac{g_4}{g_3}=-\tan(2\phi),\quad \frac{\pi}{4}<\phi\leqslant\frac{\pi}{2}, \tag{A.25}$$

so that $\theta=(l+1)\pi-2\phi$ with $l=0,1$. It should be noted that if $l=0$, i.e., $\theta=\pi-2\phi$, this results in $\theta\in[0,\pi/2)$ for $\phi\in(\pi/4,\pi/2]$ which contradicts $\theta\in(\pi/2,3\pi/2)$. Therefore, l should be equal to 1, so that $\theta=2\pi-2\phi\in[\pi,3\pi/2)\subset[0,2\pi)$ for ϕ $(\pi/4<\phi\leqslant\pi/2)$.

For sufficiently small r, the leading term $O(1/r^2)$ of the modulus of w, $w=g_3+\mathrm{i}g_4=|g_3+\mathrm{i}g_4|\mathrm{e}^{\mathrm{i}\theta}$ is obtained from (A.23), (A.24) as

$$|g_3+\mathrm{i}g_4|=\sqrt{g_3^2+g_4^2}=\frac{(3f-1)^2}{r^2}+o(r^{-2}), \tag{A.26}$$

the sine function in (A.9) becomes $\sin(\theta/2)=\sin(\pi-\phi)$, and (A.9) becomes

$$\mathrm{Im}F(x+\mathrm{i}y)=-\frac{(3f-1)y}{4(x^2+y^2)}-\frac{1}{4}\sqrt[4]{g_3^2+g_4^2}\sin(\pi-\phi)+o(r^{-2}). \tag{A.27}$$

Therefore, for small positive x, the leading order term in (A.27) has the form

$$\mathrm{Im}F(x+\mathrm{i}y) = -\frac{(3f-1)y}{4(x^2+y^2)} - \frac{1}{4}\sqrt[4]{g_3^2+g_4^2}\ \sin\phi = -\frac{(3f-1)y}{4(x^2+y^2)} - \frac{|3f-1|}{4r}\ \sin\phi. \tag{A.28}$$

We note that $\sin\phi = y/r$ and $r = \sqrt{x^2+y^2}$, so that the Dirac delta function can be written as

$$\delta(x) = \frac{1}{\pi}\lim_{y\to 0^+}\frac{y}{x^2+y^2} = \frac{1}{\pi}\lim_{y\to 0^+}\frac{\sin\phi}{r}. \tag{A.29}$$

Therefore, by substituting (A.28) into (10), and taking the limit as y approaches to 0^+, the non-negative spectral density function at the origin is obtained as

$$m(x) = \frac{3f-1}{4}\ \delta(x) + \frac{|3f-1|}{4}\ \delta(x), \quad (x\approx 0). \tag{A.30}$$

Case III: $x \approx 0$ and volume fraction $f = f_c = 1/3$. In this case, the spectral function $F(s)$ has a simple form of

$$F(s) = \frac{3}{4} - \frac{1}{4}\sqrt{9-\frac{8}{s}} \tag{A.31}$$

and (A.23), (A.24) become

$$g_3 = 9 - \frac{8\cos\phi}{r}, \quad g_4 = \frac{8\sin\phi}{r} > 0, \quad \frac{\pi}{4} < \phi \leqslant \frac{\pi}{2} \tag{A.32}$$

for sufficiently small r. For such a small r, the angle θ of the complex number $w = g_3 + \mathrm{i}g_4$ must be restricted to the interval $(0,\pi)$. (A.32) yields to

$$\lim_{r\to 0}\tan\theta = \lim_{r\to 0}\frac{g_4}{g_3} = -\tan\phi, \quad \frac{\pi}{4} < \phi \leqslant \frac{\pi}{2} \tag{A.33}$$

so that $\theta = (l+1)\pi - \phi$ with $l = 0, 1$. It should be noted that l cannot be equal to 1 because if $l = 1$, i.e., $\theta = 2\pi - \phi$, then $\theta \in [3\pi/2, 7\pi/4)$ for $\phi \in (\pi/4, \pi/2]$ which contradicts $\theta \in (0,\pi)$. Therefore, l should be equal to 0, so that $\theta = \pi - \phi$ $(\pi/4 < \phi \leqslant \pi/2)$.

For small r, the leading term $O(1/r)$ of the modulus of w, $w = g_3 + \mathrm{i}g_4 = |g_3 + \mathrm{i}g_4|\mathrm{e}^{\mathrm{i}\theta}$ can be calculated using (A.32) as

$$|g_3 + \mathrm{i}g_4| = \sqrt{g_3^2+g_4^2} = \frac{8}{r} + o(r^{-1}) \tag{A.34}$$

and (A.9) becomes

$$\mathrm{Im}F(x+\mathrm{i}y) = -\frac{1}{4}\sqrt[4]{g_3^2+g_4^2}\sin\left(\frac{\pi-\phi}{2}\right) + o\left(r^{-\frac{1}{2}}\right). \tag{A.35}$$

Therefore, for small positive x and y, the leading order term in (A.35) has the form

$$\mathrm{Im}F(x+\mathrm{i}y) = -\frac{1}{4}\sqrt[4]{g_3^2+g_4^2}\ \cos\frac{\phi}{2} + o(r^{-\frac{1}{2}}) = -\sqrt{\frac{8}{r}}\ \cos\frac{\phi}{2} + o(r^{-\frac{1}{2}}). \tag{A.36}$$

For small positive x and $r = \sqrt{x^2+y^2}$, the leading term on the right hand side of (A.36) as y goes to 0^+ is a bounded integrable function of x, i.e.,

$$m_1(x) = -\int_0^x \lim_{y\to 0^+}\mathrm{Im}F(t+\mathrm{i}y)\mathrm{d}t \leqslant \int_0^x 2\sqrt{2}t^{-\frac{1}{2}}\cos\frac{\phi}{2}\mathrm{d}t = 4\sqrt{2x}\cos\frac{\phi}{2} \leqslant 4\sqrt{2}, \tag{A.37}$$

which implies that there is no delta function at the origin in the representation of the spectral density function. From the analysis of Cases I, II and III, we conclude that (36) holds. This completes the proof of theorem. □

Remark 2. An alternative proof of Case II and Case III is given in Appendices B and C, respectively.

Appendix B. An alternative proof of Case II

Let $x = 0$, $f \neq 1/3$ and $\phi = \pi/2$ in (A.23) and (A.24), then (A.23) and (A.24) become

$$g_3 = 9 - \frac{(3f-1)^2}{y^2} < 0, \quad g_4 = \frac{6(1+f)}{y} > 0 \tag{B.1}$$

for sufficiently small positive y. Thus, the angle θ of $w = g_3 + \mathrm{i}g_4$ must be in the second quadrant, i.e., $\theta \in (\pi/2, \pi)$. Equations in (B.1) imply

$$\lim_{y\to 0^+}\tan\theta = \lim_{y\to 0^+}\frac{g_4}{g_3} = \lim_{y\to 0^+}\frac{6(1+f)y}{9y^2-(3f-1)^2} = 0^-, \tag{B.2}$$

so that $\theta = \pi^-$ or $\theta = 2\pi^-$. It should be noted that $\theta = 2\pi^-$ is not the case due to $\theta \in (\pi/2, \pi)$. Thus, the angle of the complex number $w = g_3 + ig_4$ must be $\theta = \pi^-$, and from (B.1), the modulus of w is obtained as

$$|\sqrt{g_3 + ig_4}| = \sqrt[4]{g_3^2 + g_4^2}\sin\frac{\pi^-}{2} + o(y^{-1}) = \frac{|3f-1|}{y} + o(y^{-1}) \tag{B.3}$$

for sufficiently small positive y. Therefore, (A.9) becomes

$$-\mathrm{Im}F(0+iy) = \frac{3f-1}{4y} + \frac{1}{4}\sqrt[4]{g_3^2 + g_4^2}\sin\frac{\pi^-}{2} + o(y^{-1}) = \frac{3f-1}{4y} + \frac{|3f-1|}{4y} + o(y^{-1}). \tag{B.4}$$

When $f < 1/3$, it follows from (B.4) that the spectral density function at $x = 0$ is given as

$$m(0) = -\frac{1}{\pi}\lim_{y\to 0^+} F(0+iy) = \frac{1}{\pi}\lim_{y\to 0^+}\left(\frac{3f-1}{4y} + \frac{1-3f}{4y} + o(y^{-1})\right) = 0. \tag{B.5}$$

When $f > 1/3$, noticing the spectral density formula (A.1), i.e., supp $m(x)\,dx = [x_1, x_2]$ where $0 < x_1 < x_2 < 1$ and taking the limit as y approaches to 0^+ on both sides of (B.4), we obtain, for $x \approx 0$,

$$m(x) = -\frac{1}{\pi}\lim_{y\to 0^+} F(x+iy) = \frac{3f-1}{4}\delta(x) + \frac{3f-1}{4}\delta(x) = \frac{3f-1}{2}\delta(x). \tag{B.6}$$

From (B.5) and (B.6) together with (A.1), we conclude that the spectral function $F(s)$ has the following form

$$F(s) = \frac{A_0 H(v)}{s} + \int_0^1 \frac{m(x)dx}{s-x}, \tag{B.7}$$

where $A_0 = (3f-1)/2$ and the function $H(v)$ is the Heaviside step function. This completes the proof of theorem. □

Appendix C. An alternative proof of Case III

Let $x = 0$, $f = 1/3$ and $\phi = \pi/2$. Then (A.32) reduces to

$$g_3 = 9, \quad g_4 = \frac{8}{y} \tag{C.1}$$

for sufficiently small positive y, and the angle θ of $w = g_3 + ig_4$ must be in the first quadrant, i.e., $\theta \in (0, \pi/2)$. Equations in (C.1) imply

$$\lim_{y\to 0^+}\tan\theta = \lim_{y\to 0^+}\frac{g_4}{g_3} = \frac{8}{9}\lim_{y\to 0^+}\frac{1}{y} = +\infty, \tag{C.2}$$

so that $\theta = \pi^-/2$ or $\theta = 3\pi^-/2$. It should be noted that $\theta = 3\pi^-/2$ is not the case due to $\theta \in (0, \pi/2)$. Thus, the angle of the complex number $w = g_3 + ig_4$ must be $\theta = \pi^-/2$, and from (C.1), the modulus of w is obtained as

$$|\sqrt{g_3 + ig_4}| = \sqrt[4]{g_3^2 + g_4^2} = \sqrt{\frac{8}{y}} + o(y^{-\frac{1}{2}}). \tag{C.3}$$

Therefore, (A.9) becomes

$$\mathrm{Im}F(0+iy) = -\frac{1}{4}\sqrt[4]{g_3^2 + g_4^2}\sin\frac{\theta}{2} + o(y^{-\frac{1}{2}}) = -\frac{1}{2}\sqrt{\frac{1}{y}} + o(y^{-\frac{1}{2}}). \tag{C.4}$$

Let us assume that there exists a Dirac delta function $\delta(x)$ which represents the spectral density function $m(x)$ at the origin, i.e., $m_2(x) = \delta(x)$. Then, for $f = 1/3$ and $s = x + iy$, (A.9) must have the following form

$$\mathrm{Im}F(x+iy) = \mathrm{Im}\int_0^1 \frac{\delta(x)dx}{s-x} + g(x,y) = \mathrm{Im}\left\{\frac{1}{0+iy}\right\} + g(x,y) = -\frac{1}{y} + g(x,y), \tag{C.5}$$

where $g(x,y)$ is a non-positive function which corresponds to the spectral measure at some points x away from the origin in the unit interval, i.e., $g(x,y) \to m(x)$ as y approaches to 0^+ where $0 < x < x_2$. Letting $x = 0$ in (C.5), we get

$$-\mathrm{Im}F(0+iy) = \frac{1}{y} + \text{positive function} \ \geqslant \frac{c_1}{y} \tag{C.6}$$

for some small positive y and constant $c_1 > 0$. On the other hand, by changing the sign on both sides of the Eq. (C.4), we obtain

$$-\mathrm{Im}F(0+iy) = \frac{1}{2}\sqrt{\frac{1}{y}} + o(y^{-\frac{1}{2}}) \leqslant \frac{c_2}{\sqrt{y}} \tag{C.7}$$

for some small positive y and constant $c_2 > 0$. (C.6) and (C.7) imply that the following inequality must be held:

$$\frac{c_1}{y} \leqslant -\mathrm{Im}F(0+\mathrm{i}y) \leqslant \frac{c_2}{\sqrt{y}}, \quad c_1 > 0, \quad c_2 > 0 \tag{C.8}$$

for small enough positive y. Since the inequality in (C.8) is held for all small enough positive y, we must have $c_1 = 0$, which contradicts $c_1 > 0$. We conclude that when the volume fraction is $f = 1/3$, the spectral density function cannot have delta function at the origin. This completes the proof of theorem. □

References

[1] G.A. Baker Jr., P. Graves-Morris, Padé Approximations, second ed., Cambridge University Press, 1996.
[2] S. Barabash, D. Stroud, Spectral representation for the effective macroscopic response of a polycrystal: application to third-order non-linear susceptibility, J. Phys.: Condens. Matter 11 (1999) 10323–10334.
[3] D.J. Bergman, The dielectric constant of a composite material – A problem in classical physics, Phys. Rep. C 43 (1978) 377–407.
[4] D.J. Bergman, Rigorous bounds for the dielectric constant of a two-component composite, Ann. Phys. 138 (1982) 78.
[5] D.J. Bergman, Hierarchies of Stieltjes functions and their application to the calculation of bounds for the dielectric constant, SIAM J. Appl. Math. 53 (4) (1993) 915–930.
[6] D.A.G. Bruggemann, Berechnung verschiedener physikalischer Konstanten von heterogen Substanzen, Ann. Phys. 24 (1935) 636–679.
[7] C. Bonifasi-Lista, E. Cherkaev, Analytical relations between effective material properties and microporosity: application to bone mechanics, Int. J. Eng. Sci. 46 (2008) 1239–1252.
[8] C. Bonifasi-Lista, E. Cherkaev, Electrical impedance spectroscopy as a potential tool for recovering bone porosity, Phys. Med. Biol. 54 (10) (2009) 3063–3082.
[9] E. Cherkaev, K.M. Golden, Inverse bounds for microstructural parameters of a composite media derived from complex permittivity measurements, Waves in Random Media 8 (1998) 437–450.
[10] E. Cherkaev, Inverse homogenization for evaluation of effective properties of a mixture, Inverse Prob. 17 (2001) 1203–1218.
[11] E. Cherkaev, D. Zhang, Coupling of the effective properties of a random mixture through the reconstructed spectral representation, ETOPIM Proc. Phys. B: Phys. Conden. Matter 338 (2003) 16–23.
[12] A.R. Day, M.F. Thorpe, The spectral function of a composite: the inverse problem, J. Phys. Condens. Matter 11 (1999) 2551–2568.
[13] A.R. Day, M.F. Thorpe, A.R. Grant, A.J. Sievers, The spectral function of a composite from reflectance data, Phys. B 279 (2000) 17–20.
[14] M. Gajdardziska-Josifovska, R.C. McPhedran, D.J.H. Cockayne, D.R. McKenzie, R.E. Collins, Silver-magnesium fluoride cermet films. (1) preparation and microstructure, (2) Optical and electrical properties, Applied Optics, (1) 28 (14) (1989) 2736–2743; (2) 28 (14) (1989) 2744–2753.
[15] K. Ghosh, R. Fuchs, Spectral theory for two-component porous media, Phys. Rev. B 38 (8) (1988) 5222–5236.
[16] K. Ghosh, R. Fuchs, Critical behavior in the dielectric properties of random self-similar composites, Phys. Rev. B 44 (14) (1991) 7330–7343.
[17] K. Golden, G. Papanicolaou, Bounds on effective parameters of heterogeneous media by analytic continuation, Commun. Math. Phys. 90 (1983) 473–491.
[18] A.V. Goncharenko, Generlization of the Bruggeman equation and a concept of shape-distributed particle composites, Phys. Rev. E 68 (4) (2003) 04118.
[19] A.V. Goncharenko, Y. Chang, Effective dielectric properties of biological cells: Generalization of the spectral density function approach, J. Phys. Chem. B. 113 (2009) 9924–9931.
[20] J.D. Jackson, Classical Electrodynamics, Wiley, New York, NY, 1975.
[21] Y. Kantor, D.J. Bergman, The optical properties of cerments from the theory of electrostatic resonances, J. Phys. C: Solid State Phys. 15 (1982) 2033–2042.
[22] R. Landauer, The electrical resistance of binary metallic mixtures, J. Appl. Phys 23 (7) (1952) 779–784.
[23] H. Ma, R. Xiao, P. Sheng, Third order optical nonlinearity enhancement through composite microstructures, J. Opt. Soc. Am. B 15 (3) (1998) 1022–1029.
[24] R.C. McPhedran, D.R. McKenzie, G.W. Milton, Extraction of structural information from measured transport properties of composites, Appl. Phys. A 29 (1982) 19–27.
[25] R.C. McPhedran, G.W. Milton, Inverse transport problems for composite media, Mat. Res. Soc. Symp. Proc. 195 (1990) 257–274.
[26] G.W. Milton, Bounds on the complex dielectric constant of a composite material, Appl. Phys. Lett. 37 (3) (1980) 300–302.
[27] G.W. Milton, The coherent potential approximation is a realizable effective medium scheme, Commun. Math. Phys. 99 (4) (1985) 463–500.
[28] G.W. Milton, Theory of Composites, Cambridge University Press, 2002.
[29] A.V. Osipov, K.N. Rozanov, N.A. Simonov, S.N. Starostenko, Reconstruction of intrinsic parameters of a composite from the measured frequency dependence of permeability, J. Phys.: Condens. Matter 14 (2002) 9507–9523.
[30] G. Ruossy, E. Spaak, J.M. Thiebaut, Universal equation for the effective complex permittivity of mixtures valid for dielectric–dielectric and dielectric-conductor mixtures, Phys. Rev. B 46 (1992) 11452–11455.
[31] A. Sihvola, Electromagnetic mixing formulas and applications, IEE Elect. Waves Ser. Inst. Elect. Eng. Lond. 47 (1999).
[32] J. Sturm, P. Grosse, W. Theiß, Effective dielectric functions of alkali halide composites and their spectral representation, Z. Phys. B-Condens. Matter 83 (1991) 361–365.
[33] A.N. Tikhonov, V.Y. Arsenin, Solutions of Ill-Posed Problems, Willey, New York, 1977.
[34] S. Torquato, S. Hyun, Effective-medium approximation for composite media: Realizable single-scale dispersions, J. Appl. Phys. 89 (3) (2001) 1725–1729.
[35] A.P. Vinogradov, A.V. Dorofeenko, S. Zouhdi, On the problem of the effective parameters of metamaterials, Phys.-Uspekhi 51 (5) (2008) 485–492.
[36] K.P. Yuen, M.F. Law, K.W. Yu, P. Sheng, Enhancing of optical nonlinearity through anisotropic microstructures, Optics Commun. 148 (1998) 197–207.
[37] D.V. Widder, The Laplace Transform, Princeton University Press, 1946.
[38] D. Zhang, E. Cherkaev, Padé approximations for identification of air bubble volume from temperature or frequency dependent permittivity of a two-component mixture, Inverse Prob. Sci. Eng. 16 (4) (2008) 425–445.
[39] D. Zhang, E. Cherkaev, Reconstruction of spectral function from effective permittivity of a composite material using rational function approximations, J. Comput. Phys. 228 (2009) 5390–5409.
[40] D. Zhang, M.P. Lamoureux, G.F. Margrave, E. Cherkaev, Rational approximation for estimation of quality Q-factor and phase velocity in linear, viscoelastic, isotropic media, Comput. Geosci. 15 (1) (2011) 117–133.